

Article

A Comprehensive Optimization Model of Tooth Surface Parameters for the Minimization of Contact Stress of Helical Face Gears by Considering the Avoidance of Edge Contact

Shenghui Wang^{1,2}, Bo Hu^{1,2} , Zhenyu Wu^{1,2,3}, Yuansheng Zhou^{1,2,*}  and Jinyuan Tang^{1,2}¹ College of Mechanical and Electrical Engineering, Central South University, Changsha 410083, China² State Key Laboratory of High Performance Complex Manufacturing, Central South University, Changsha 410083, China³ School of Mechatronics Engineering, Guizhou Minzu University, Guiyang 550025, China

* Correspondence: zyszby@csu.edu.cn

Abstract: Optimization with edge contact avoidance and contact stress minimization is essential for gear design. Due to the complex geometry of modified helical face gear drives, it is complicated to find the optimal design parameters with the consideration of issues including loading, assembly errors, and edge contact. As the finite element method is tedious and time-consuming, an optimization model with a simplified algorithm of the loaded tooth contact analysis with errors (ELTCA) for modified helical face gears is presented, and it can programmatically optimize the contact stress with edge contact avoidance. Firstly, a simplified ETCA algorithm is introduced, which reduces the five unknowns in the traditional contact equations to three. Secondly, the LTCA is analytically implemented according to the Hertz theory. Subsequently, an optimization model with the objective function of avoiding edge contact and reducing maximum contact stress is proposed. Furthermore, the proposed model is applied to reveal the effects of design parameters and assembly errors on the optimized contact path and stress. The results show that the optimization model is accurate and efficient; the design parameters and assembly errors have great effects on the meshing of modified helical face gears.

Keywords: design optimization; edge contact; contact stress; modified helical face gear; loaded tooth contact analysis with errors (ELTCA)

MSC: 65E05

Citation: Wang, S.; Hu, B.; Wu, Z.; Zhou, Y.; Tang, J. A Comprehensive Optimization Model of Tooth Surface Parameters for the Minimization of Contact Stress of Helical Face Gears by Considering the Avoidance of Edge Contact. *Mathematics* **2022**, *10*, 3102. <https://doi.org/10.3390/math10173102>

Received: 27 July 2022

Accepted: 25 August 2022

Published: 29 August 2022

Publisher's Note: MDPI stays neutral with regard to jurisdictional claims in published maps and institutional affiliations.



Copyright: © 2022 by the authors. Licensee MDPI, Basel, Switzerland. This article is an open access article distributed under the terms and conditions of the Creative Commons Attribution (CC BY) license (<https://creativecommons.org/licenses/by/4.0/>).

1. Introduction

Face gear drives have wide application prospects under the working conditions of high speed and heavy loads, such as the transmission systems in helicopters and machine tools, owing to their small size, light weight, low noise, large capacity, and high reliability. The transmission performances of face gears are closely related to many factors, such as design, manufacture, and installation. However, edge contact, contact area distribution, and maximum contact stress can restrict the service life of face gears. Unfortunately, current gear design methods, including finite element analysis (FEA) and numerical tooth contact analysis (TCA), do not automatically identify edge contact and minimize the maximum contact stress, despite the complexity of the process and the high technical experience requirements of the personnel. Namely, the automatic comparison and optimization of gear design parameters cannot be realized at present. Therefore, under the condition without repeated modeling, determining how to automatically avoid edge contact, quickly calculate the optimal maximum contact stress, output the optimal design parameters, and show the qualified contact path is of great significance.

In terms of the research on face gear geometry design, many publications can be referred to. Litvin et al. made outstanding contributions to the theory and application

of face gears. They deduced the surface equations of the standard face gear [1] and the face gear with offset [2]; introduced the FEA method of stress analysis [3–6]; presented the theory of spur face gears in a handbook [7]; and summarized the technologies of gears, including face gears, in a book [8]. Their work provides significant references for researchers in the field of gears. In addition, Zhou et al. presented a new closed-form model for the geometry establishment of face gears without solving nonlinear equations [9], and the model was applied to the modeling and milling of face gears [10–15]. In addition, they put forward a time-saving CAD/CAE integration method [16,17] for optimizing design parameters with FEA. Liu et al. [18] proposed a new type of face gear drive that can achieve non-uniform transmission ratios. This face gear drive, which consists of an undulating face gear and a planar noncircular gear, is applied to transmit the angular velocity of change. Zschippang et al. [19] elaborated a general method for the generation of face gears with shaft angle, helical angle, and axial offset. In addition, they described the procedure for determining geometry quality. Tan [20–22] studied the face gear that meshes with a conical involute pinion and discussed the generation and geometry modeling methods with the conditions of gear integrity obtained. In order to investigate the strength variation of face gears, Li et al. [23] constructed an equivalent face gear based on ISO 6336 standard. Lin et al. [24] researched a non-circular face gear pair and established multiple analytical models and equations for the classification of transmission patterns, transmission ratios, and relative motions. Moreover, Lin [25] also provided a discrete algorithm for the curve-face gear pair and analyzed the limiting points in the determination rule. Zhang et al. [26] investigated the tooth geometry and contact characteristics of offset-axis face gear drives in detail by simulating the conjugate motion. Guo et al. [27] simulated the computerized generation of face gear drives enveloped by circular cutters.

For the purpose of improving the contact performances of face gear drives, the methods of profile modification are applied in geometry design. Litvin et al. [28] investigated two kinds of face gear drives generated by modified shapers, including the design, generation, and stress analysis. They also compared the contact stress of the two kinds of modified face gears. Meanwhile, they proposed the modification geometry of an asymmetric face gear and applied a tooth contact analysis (TCA) algorithm to calculate the contact path, which was verified by the FEA method [29]. Furthermore, they analyzed a helical face gear that was enveloped by two mismatched parabolic racks corresponding to the pinion and the shaper from the aspects of design, generation, and stress analysis. Wu et al. [30] established a model of a parabolically modified face gear to perform TCA and researched the factors affecting the meshing path. Moreover, they obtained the ideal position of the contact area. For the aim of investigating the behavior of a transmission composed of a face gear and a modified pinion, Barone et al. [31] established geometric models based on enveloping theory and applied FEA models for simulation. Peng et al. [32] provided the ease-off surface modification to the manufacturing process of face gears to control the unloaded meshing performance. To reduce the sensitivity of the modified face gear drive to misalignments, Zanzi et al. [33] worked on an enhanced approach of longitudinal plunging to generate a double-crowned face gear drive.

Transmission systems composed of face gears are also investigated by scholars. Dong et al. explored the characteristics of concentric face gear split-torque transmission systems, for instance, the assembly conditions, power flow directions, load sharing performances [34], and the method of mesh stiffness calculation [35]. Mo et al. [36] conducted an investigation on the load sharing of a power-split system that consists of face gears by using an analytical method, and the investigation method was applied to study a herringbone planetary gear system that contains a floating sun gear and flexible support [37].

However, the above studies on TCA of face gears are based on the existing commercial software for FEA [38], or the traditional analytical TCA model is used to solve the coordinates of contact points. The FEA method not only is time-consuming and may result in unstable convergence, but also often requires repeated manual modeling work. As the traditional TCA model is used to calculate the contact points of the tooth

surface analytically, the solution of multiple equations is too complex and the stability is poor. Moreover, neither of the two methods can automatically identify and avoid the edge contact, achieve the parametric optimization of the maximum contact stress of the tooth surface, or automatically return the final optimized design parameters. The research on helical face gears, especially the modified helical ones, is not involved numerically.

In this paper, a simplified algorithm of the tooth contact analysis with errors (ETCA) of modified helical face gears is provided [14], based on which an automatic optimization algorithm of the loaded tooth contact analysis with errors (ELTCA) that integrates the functions of contact stress optimization and edge contact avoidance is proposed. Firstly, an ETCA algorithm, derived from the traditional algorithm by simplifying the contact equations and solving the rotation angles of gears separately, is introduced. Secondly, the coordinates of contact points are obtained with the ETCA algorithm. The geometric parameters, such as the contact ellipses and curvatures of the contact points, are calculated based on the coordinates, and the ELTCA algorithm is presented according to the Hertz theory to calculate the contact stress. The effectiveness of the ELTCA algorithm is verified through comparison with the finite element simulation. Furthermore, the optimization model considering the edge contact avoidance and the minimization of maximum contact stress is established, and it is verified based on the simplified ELTCA algorithm. Finally, the influence of the geometric parameters and assembly errors on the contact path and the maximum contact stress is explored by applying the optimization model.

2. A Simplified ETCA Algorithm of Modified Helical Face Gears

2.1. Description of the Tooth Surface and Basic Coordinate Systems

As illustrated in Figure 1a, the modified tooth surface of shaper r_s and tooth surface of pinion r_1 are generated by rack cutters with parabolic modification. Likewise, the tooth surface of modified helical face gear r_{2w} is generated by the shaper [28], as shown in Figure 1b. The face gear and the pinion rotate around the intersected axes at angular velocities ω_2 and ω_1 , respectively. Additionally, the shaft angle is γ_m and the helix angle is β . In coordinate system S_r in Figure 1a, the vertex of the parabola is point P_0 , which is determined by the distance l_d and the parameter u_0 . l_d is calculated as $0.5s_0 \cdot \cos\alpha_n$. The quadratic coefficient of the parabola is a_r , the pressure angle is α_n , and the width of the rack cutter in the normal section is s_0 . In addition, r_p is the reference radius of the shaper, and φ_1 and φ_s are the rotation angles of the pinion and the shaper, respectively, in the generation progress. P_r is a moving point on the profile of the rack cutter.

According to the method in [8], the closed-form tooth surface equation of the modified helical face gear can be presented as

$$\begin{cases} \mathbf{r}_{2w}(u_r, \varphi_s, u_z(u_r, \varphi_s)) = \mathbf{M}_{2s}(\varphi_s) \cdot \mathbf{r}_s(u_r, u_z(u_r, \varphi_s)) \\ u_z(u_r, \varphi_s) = \frac{[(\boldsymbol{\omega}_2 - \boldsymbol{\omega}_s) \times \mathbf{o}_s \mathbf{q}_u(u_r)] \cdot \mathbf{N}(u_r)}{[(\boldsymbol{\omega}_2 - \boldsymbol{\omega}_s) \times \mathbf{I}_s] \cdot \mathbf{N}(u_r)} \end{cases} \quad (1)$$

where u_r is the rack profile parameter, u_z is the distance along the z-axis direction, $\boldsymbol{\omega}_s$ is the angular velocity of the shaper, \mathbf{I}_s is the unit vector of the shaper in the axis direction, and $\mathbf{o}_s \mathbf{q}_u$ is the distance vector from the coordinate origin \mathbf{o}_s to any point on the shaper end profile.

Considering that the TCA in this paper contains assembly errors, the error coordinate system is introduced as shown in Figure 2. The coordinate system $S_1(x_1, y_1, z_1)$ is rigidly connected to the pinion. $S_q(x_q, y_q, z_q)$, $S_e(x_e, y_e, z_e)$ and $S_d(x_d, y_d, z_d)$ are auxiliary coordinate systems. $\Delta\gamma_m$ is the error of shaft angle, ΔE is the offset error of the pinion, and Δq is the axial displacement error of the face gear. φ_1 and φ_2 are the rotation angles of the pinion and the face gear, respectively. As shown in Figure 2a, the transformation matrix from the coordinate system S_1 to S_f is \mathbf{M}_{f1} . The transformation matrix from coordinate system S_2 to S_f is \mathbf{M}_{f2} . For the sake of simplification, the submatrices of \mathbf{M}_{f1} and \mathbf{M}_{f2} are represented by \mathbf{T}_{f1} and \mathbf{T}_{f2} , respectively. The center distance between the shaper and the pinion is B , the

expression of which is $m_n(Z_s - Z_1)/(2\cos\beta)$; m_n is the normal module, and Z_1 and Z_s are the tooth numbers of the shaper and the pinion, respectively.

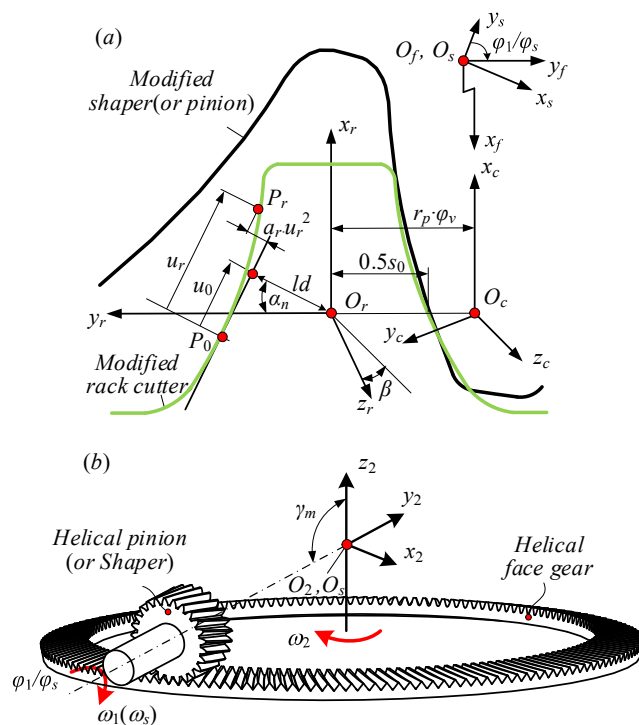


Figure 1. Generation process diagrams of modified helical face gears: (a) modified rack cutters envelop modified shapers; (b) helical gears envelop helical face gears.

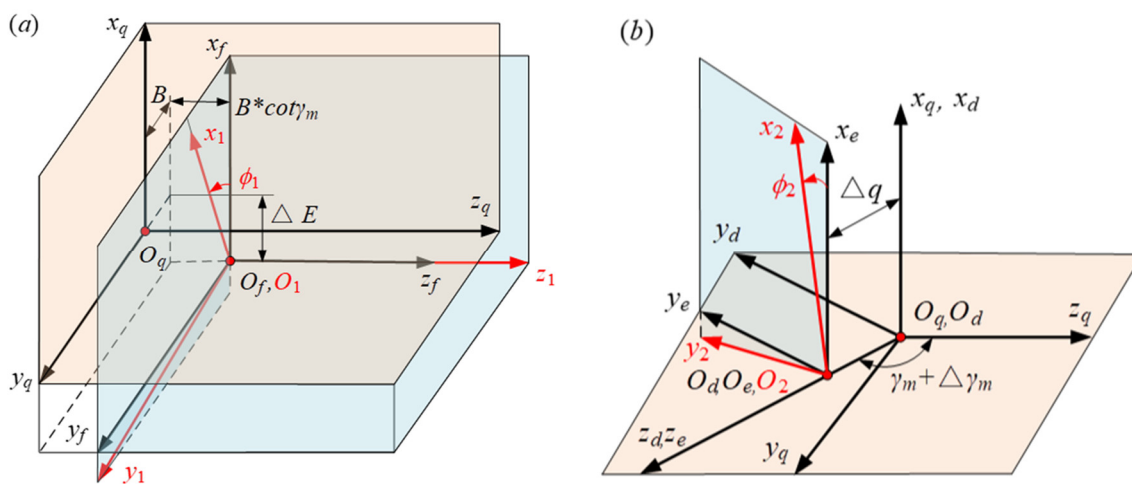


Figure 2. The coordinate system with assembly errors in ETCA: (a) the coordinate system with ΔE ; (b) the coordinate system with Δq and $\Delta \gamma_m$.

2.2. The Simplified ETCA Algorithm

The simplified ETCA algorithm is realized by deriving the representations of the rotational angles of the two gears in advance and reducing the number of unknowns in contact equations. Compared with the traditional ETCA algorithm, the algorithm has various advantages in terms of computational efficiency and convergence [14].

In Figure 3a, the axes of the pinion and the face gear are L_1 and L_2 , respectively. Σ_1 and Σ_2 represent the tooth surfaces of the pinion and the face gear, respectively. The unit axis vectors of the pinion and the face gear are l_1 and l_2 , respectively, as shown in Figure 3b.

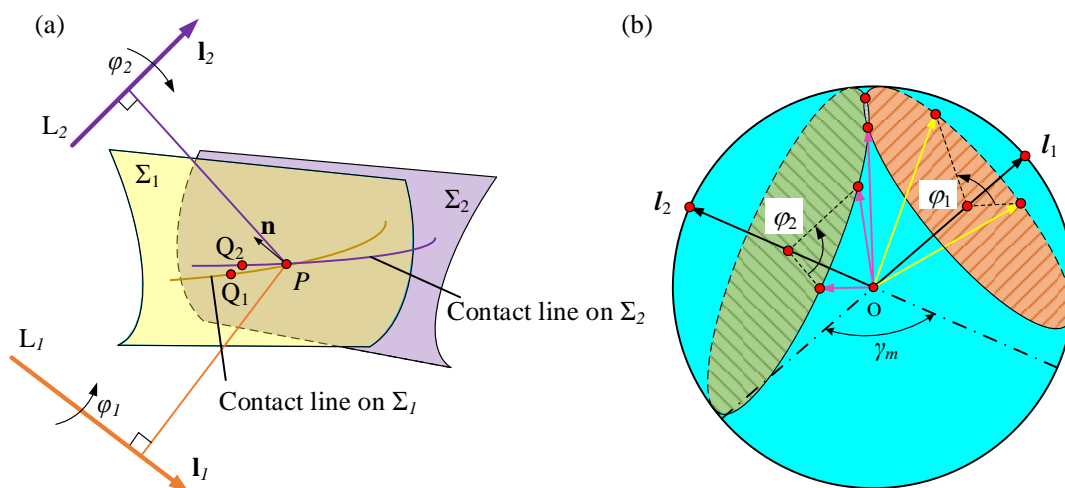


Figure 3. Geometrical relationship of the contact point: (a) contact point; (b) normal vector.

The unit normal vector of point Q_1 on the pinion surface is $\mathbf{n}^{(1)}$, which is \mathbf{n}_{Q1} in Figure 3b. The angle between the normal vector and the pinion axis is

$$\alpha_1 = a \cos(\mathbf{n}_{Q1} \cdot \mathbf{l}_1) = a \cos(\mathbf{n}^{(1)} \cdot \mathbf{l}_1) \tag{2}$$

The point Q_1 rotates around the axis L_1 at angle φ_1 and arrives at point P , the unit normal vector of which is (as shown in Figure 3b)

$$\begin{aligned} \mathbf{n}_{r1} &= \mathbf{b}_1 + \mathbf{b}_2 \cdot \cos \varphi_1 + \mathbf{b}_3 \cdot \sin \varphi_1 \\ \mathbf{b}_1 &= (\mathbf{n}^{(1)} \cdot \mathbf{l}_1)(1 - \cos \varphi_1)\mathbf{l}_1 \\ \mathbf{b}_2 &= \mathbf{n}^{(1)} \\ \mathbf{b}_3 &= \mathbf{l}_1 \times \mathbf{n}^{(1)} \end{aligned} \tag{3}$$

Similarly, the unit normal vector of point Q_2 on Σ_2 is $\mathbf{n}^{(2)}$, which is \mathbf{n}_{Q2} in Figure 3b.

According to the relationship of geometry, the angle between axis L_1 and the normal vector of point P on surface Σ_2 needs to meet the constraint that is

$$\mathbf{n}_{r2} \cdot \mathbf{l}_1 = \cos \alpha_1 \tag{4}$$

Then, angle φ_2 can be obtained as

$$\begin{aligned} \varphi_2 &= a \sin(\cos \alpha_1 - (\mathbf{n}^{(2)} \cdot \mathbf{l}_2) \cdot \mathbf{l}_1 \cdot \mathbf{l}_2) - \varphi'_2 \\ \varphi'_2 &= a \tan 2(\mathbf{b}_2 \cdot \mathbf{l}_1 - (\mathbf{n}^{(2)} \cdot \mathbf{l}_2) \cdot \mathbf{l}_1 \cdot \mathbf{l}_2, \mathbf{b}_3 \cdot \mathbf{l}_1) \end{aligned} \tag{5}$$

Therefore, the six equations with six unknowns in traditional contact equations can be simplified as

$$\begin{cases} \mathbf{r}_{fx}^{(1)}(u_{r1}, \varphi_1(u_{r1}, \varphi_s)) = \mathbf{r}_{fx}^{(2)}(u_r, \varphi_s, \varphi_2(u_r, \varphi_s)) \\ \mathbf{r}_{fy}^{(1)}(u_{r1}, \varphi_1(u_{r1}, \varphi_s)) = \mathbf{r}_{fy}^{(2)}(u_r, \varphi_s, \varphi_2(u_r, \varphi_s)) \\ \mathbf{r}_{fz}^{(1)}(u_{r1}, \varphi_1(u_{r1}, \varphi_s)) = \mathbf{r}_{fz}^{(2)}(u_r, \varphi_s, \varphi_2(u_r, \varphi_s)) \end{cases} \tag{6}$$

3. ELTCA of Helical Face Gears Based on the Simplified ETCA Algorithm

3.1. The Contact Ellipse and Contact Stress

As illustrated in Figure 4a, Σ_1 and Σ_2 represent the undeformed surfaces of the pinion and the face gear, respectively. As the normal force F_n is applied on the tooth surfaces, Σ_1 and Σ_2 will deform and move to $\Sigma_{1'}$ and $\Sigma_{2'}$. Meanwhile, point Z_1 on Σ_1 has the normal

displacement u_1 , and point Z_2 on Σ_2 has the normal displacement u_2 . δ_1 and δ_2 are the elastic deformations of the tooth surfaces Σ_1 and Σ_2 on the contact point, respectively, and their sum δ is the total deformation.

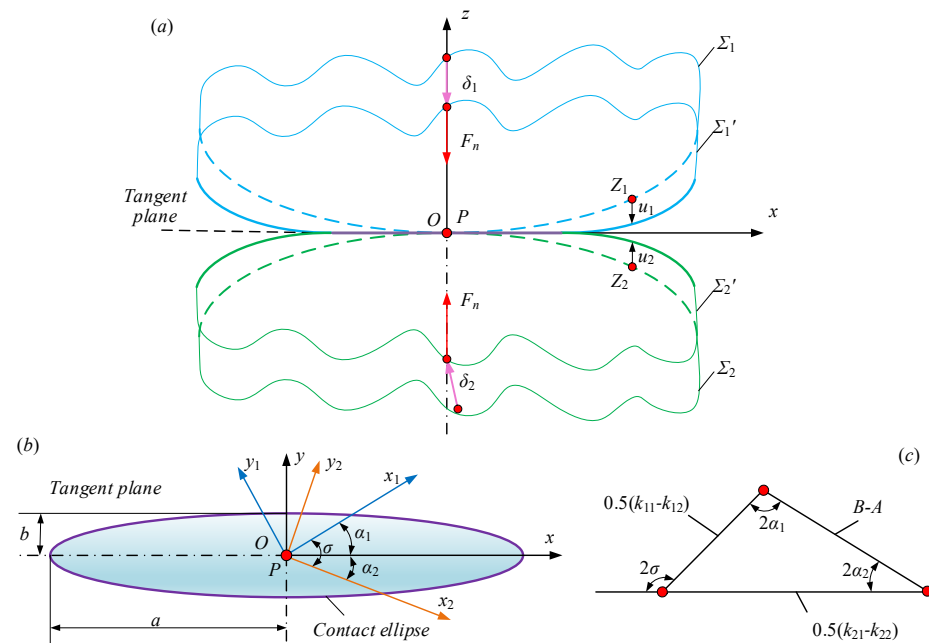


Figure 4. The elastic deformation of the contact point: (a) deformation diagram; (b) contact ellipse; (c) curvature relationship.

Additionally, the contact point P in the tangent plane turns into an elliptical area due to the elastic deformation, and point P is still the center of the ellipse. As shown in Figure 4b,c, x_1 and x_2 are the principal directions, and the angle between the two directions is σ . k_{i1} ($i = 1, 2$) and k_{i2} are the principal curvatures of the tooth surface Σ_i at the point P . Hertz deduced the formulas of the semi-major axis and the semi-minor axis [39] as follows:

$$\begin{aligned}
 a &= \left(\frac{1}{E^*} \cdot \frac{3F_n}{2\pi W} \cdot \frac{1}{e^2} \cdot [K(e) - E(e)] \right)^{1/3} \\
 b &= a\sqrt{1 - e^2}
 \end{aligned}
 \tag{7}$$

where e is the eccentricity. E^* is the equivalent elastic modulus that can be expressed by Poisson's ratios ν_1 and ν_2 as well as the elastic moduli E_1 and E_2 of the materials of two gears. $K(e)$ and $E(e)$ are the first and second elliptic integrals, respectively. W is a positive constant:

$$\begin{aligned}
 W &= 0.25 \cdot (k_{11} + k_{12} + k_{21} + k_{22}) \\
 &\quad - 0.25 \cdot [(k_{11} - k_{12})^2 + (k_{21} - k_{22})^2 \\
 &\quad + 2 \cdot (k_{11} - k_{12})(k_{21} - k_{22}) \cos 2\sigma]^{1/2}
 \end{aligned}
 \tag{8}$$

The maximum contact stress is

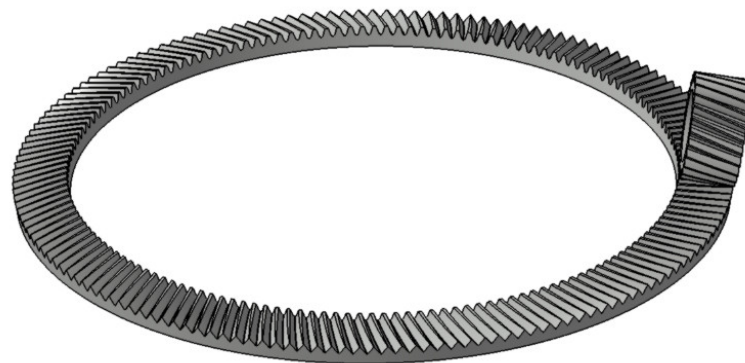
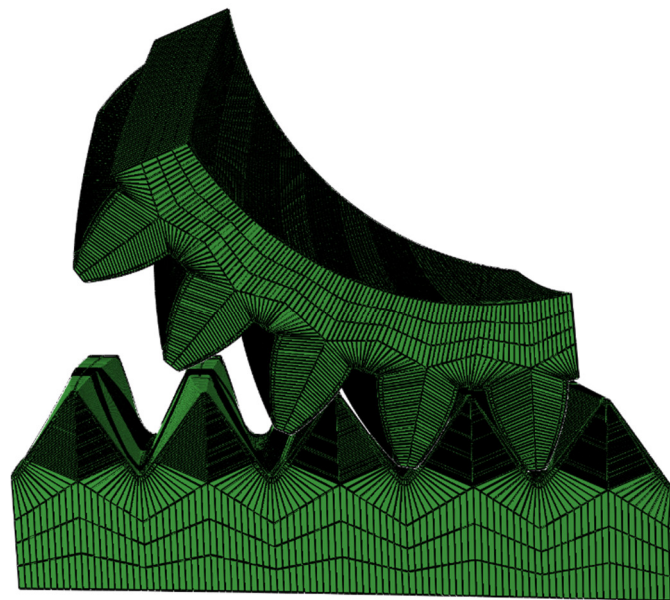
$$P_0 = \frac{3F_n}{2\pi \cdot a \cdot b}
 \tag{9}$$

3.2. Validation of the Simplified ELTCA Algorithm

In this section, the proposed ELTCA algorithm is compared with the finite element simulation based on commercial software to verify the contact path, contact area, and contact stress. The basic design parameters of the modified helical face gear are shown in Table 1. The established 3D model of the modified helical face gear drive is shown in Figure 5, and the five-tooth model of the finite element simulation is shown in Figure 6.

Table 1. Basic design parameters of a helical face gear drive.

Parameter	Value
Normal module m_n (mm)	6.35
Tooth number of pinion Z_1	25
Tooth number of face gear Z_2	160
Tooth number of shaper Z_s	28
Pressure angle α_n ($^\circ$)	25
Shaft angle γ_m ($^\circ$)	100
Helical angle β ($^\circ$)	15
The outer radius of face gear L_2 (mm)	600
The inner radius of face gear L_1 (mm)	510

**Figure 5.** A 3D model of the modified helical face gear transmission.**Figure 6.** Five-tooth model of finite element simulation.

The parameter u_0 is set as 1.2 mm, and the parameter a_r is equal to 0. Both the pinion and the face gear are made of steel material with the properties of the elasticity modulus $E = 2.068 \times 10^5$ N/mm² and Poisson's ratio $\nu = 0.29$. The face gear forced by a load torque $T = 1600$ N·m is driven by the pinion.

The contact area obtained by finite element simulation is shown in Figure 7, and the contact area calculated by the ELTCA model in this paper is shown in Figure 8. The contact stress comparisons obtained by the two methods are shown in Table 2.

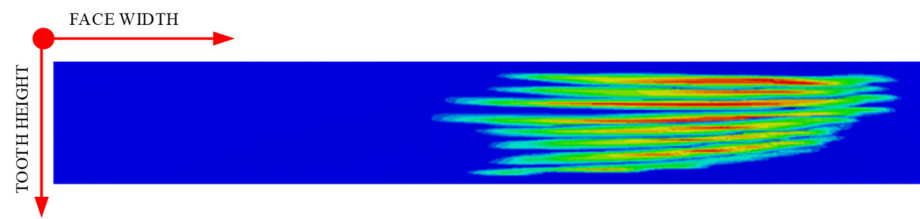


Figure 7. Stress nephogram in finite element simulation (red: maximum contact stress).

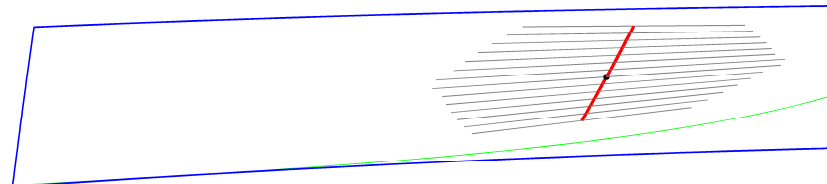


Figure 8. The contact area calculated by the ELTCA algorithm.

Table 2. Contact stress comparison between the finite element simulation and the ELTCA.

Contact Point Number	Long Axes a /Short Axes b (mm)	Analytical Stress Value (MPa)	Finite Element Method Stress Value (MPa)	Relative Error (%)
1	22.956016/0.579899	799.23	707.4	11.49
2	22.968336/0.570494	812.07	724.9	10.73
3	22.983611/0.560628	825.91	749.4	9.26
4	23.001982/0.550285	840.87	762.8	9.28
5	23.023616/0.539449	857.08	778.6	9.15
6	23.048712/0.528098	874.69	788.7	9.83
7	23.077492/0.516207	893.88	803.8	10.07
8	23.110200/0.503753	914.86	806.1	11.89
9	23.147144/0.490703	937.89	828.2	11.69
10	23.188683/0.477022	963.29	838.3	12.97
11	23.235227/0.462669	991.45	895.5	9.67
12	23.287283/0.447597	1022.86	992.4	2.97
13	23.345481/0.431744	1058.16	1148	−8.49

Figures 7 and 8 show that the contact areas obtained by the two methods are basically the same, and the contact paths formed by instantaneous maximum contact stress points are also consistent. As shown in Table 2, the contact stresses of the 13 contact points calculated by the analytical method and the finite element simulation are close to each other numerically. The maximum relative error between the two methods is 12.97%; since the influence of the wheel body, web, and other structures is not considered here, the calculation accuracy of the ELTCA algorithm is acceptable.

4. A Comprehensive Optimization Model of the Contact Stress Based on the Simplified ELTCA

4.1. The Optimization Model of the Contact Stress

In the Hertz theory, the maximum contact stress is formulated as Equation (9). However, this formula is not suitable for the case of edge contact, nor can it be applied to optimize the contact calculation, for example by filtering tooth surface parameters and reducing the maximum contact stress.

The optimization model is proposed based on the following ideas:

- (i) The edge contact should be avoided.
- (ii) The maximum contact stress should be minimized by optimizing the modification parameters.

As shown in Figure 9a, point P_{IJ} ($I \in [1, M], J \in [1, N]$) is sampled from the cross-section of the face gear blank, and the sampling points correspond to the $M \times N$ points on the tooth surface of the modified helical face gear.

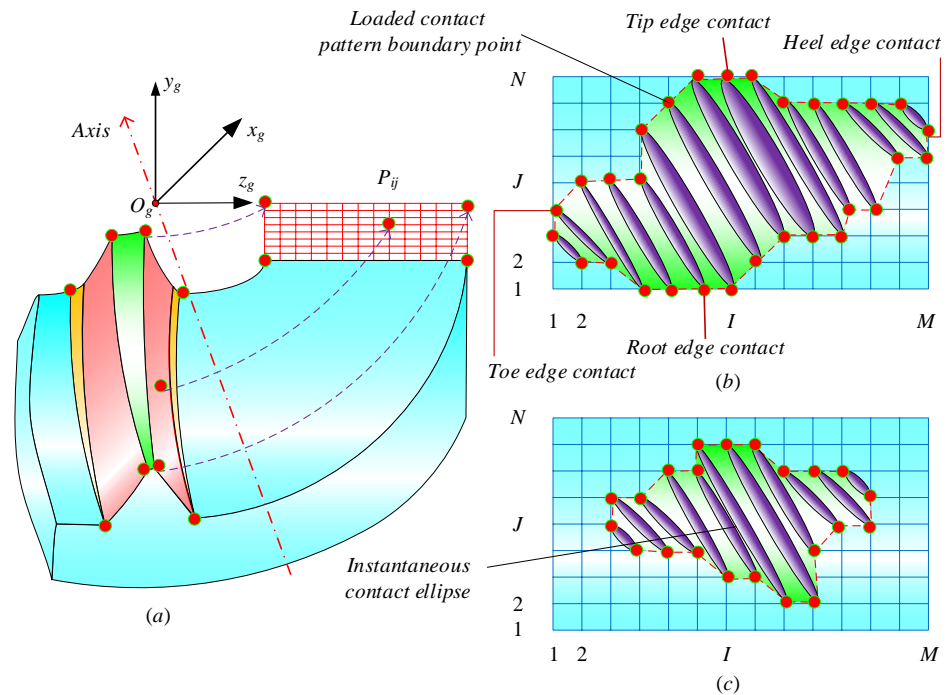


Figure 9. Tooth surface discretization and loaded contact pattern evaluation: (a) discretized points; (b) contact pattern with edge contact; (c) acceptable loaded contact pattern.

If edge contact occurs (as shown in Figure 9b), at least one point will fall on the boundary line of tooth surfaces. Accordingly, the value of I is equal to M , or the value of J is equal to N . For purpose of avoiding edge contact, the following restrictions should be met.

$$\begin{aligned}
 \text{s.t. } & 1 < I^* < M \\
 & 1 < J^* < N
 \end{aligned}
 \tag{10}$$

The objective function of contact stress optimization is to minimize the value of contact stress. Based on the constraints in Equation (10), the optimal load contact pattern (LCP) can be simulated automatically in the program through cyclic comparison so that the corresponding optimization parameters a_{rM} and u_{0M} can be calculated. The optimization model is formulated as

$$\begin{aligned}
 f(a_r, u_0) &= \frac{3Fn}{2\pi a(a_r, u_0)b(a_r, u_0)} \\
 (a_{rM}, u_{0M}) &= \arg \min f(a_r, u_0)
 \end{aligned}
 \tag{11}$$

Finally, according to the optimal modification coefficients a_{rM} and u_{0M} , the contact stress can be calculated as

$$f(a_{rM}, u_{0M}) = \frac{3Fn}{2\pi a(a_{rM}, u_{0M})b(a_{rM}, u_{0M})}
 \tag{12}$$

To realize the programming of the optimization algorithm, the global optimization algorithm that integrates the grid searching with the downhill simplex method is employed in the solving process. The solving procedure can be summarized in the following steps as demonstrated in Figure 10.

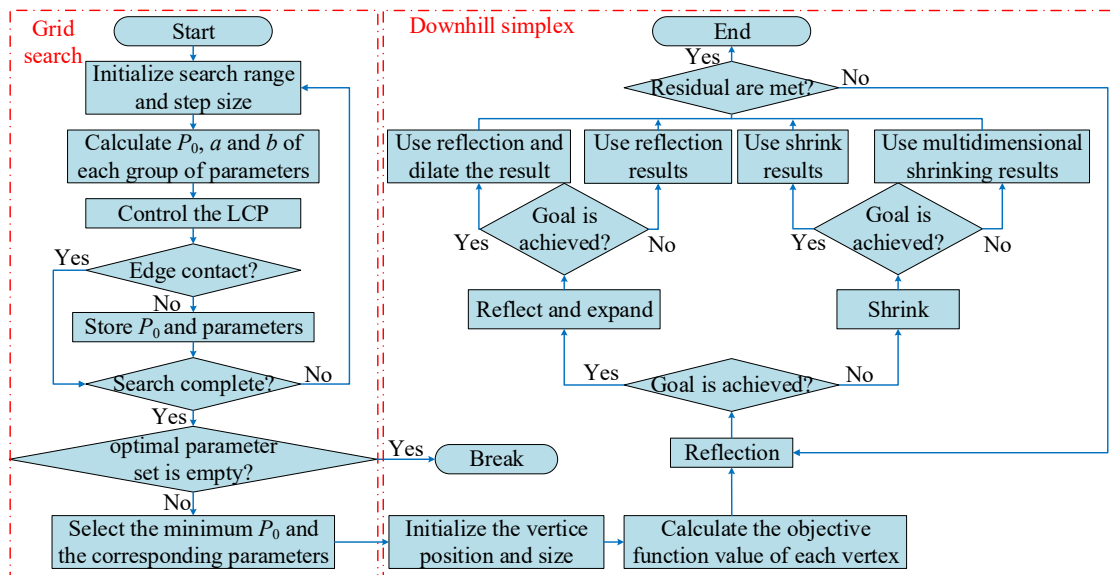


Figure 10. Flow chart of the optimization algorithm.

Step 1 is to initialize the search range and the step size in grid searching. The search range of the parabolic offset distance is set as $u_0 \in [-1, 2]$, and the step size is 0.1. The search range of the parabolic coefficient is set as $a_r \in [-0.01, 0.01]$, and the step size is 0.001.

Step 2 is to calculate the objective function of modification parameters in each group as well as store the value of the function and corresponding parameters that meet the constraints of Equation (10). A group of modification parameters that minimize the value of the objective function is selected as the initial value of the optimization algorithm of the downhill simplex.

Step 3 is to initialize the position and the size of simplex vertices. The initial size of the simplex is set as 0.1, and the number of iterations is set as 40.

Step 4 is to calculate the objective function value of each simplex vertex. Through four methods of reflection, reflection and expansion, contraction, and multidimensional contraction, new vertices are obtained to form a new simplex by replacing the worst point in the original simplex.

Step 5 is to repeat **Step 4** until the residual requirements are met.

4.2. Contact Path and Contact Stress Calculation Based on the Optimization Model

The basic design parameters of the helical face gear drive in this section are the same as those in Section 3.2. As described in Section 4.1, the two coefficients u_0 and a_r that determine the geometry of the parabola of the modified shaper are the main optimization parameters. Within the given intervals of the modification coefficients $u_0 \in [-1, 2]$ and $a_r \in [-0.01, 0.01]$, the calculated optimal parameters as well as the minimum value of the maximum contact stress are presented in Table 3.

The minimum value of the maximum contact stress is 758.36 Mpa and is shown as a black point in Figure 11, the corresponding parameter u_0 which determines the position of the parabola apex is 1.6406 mm, and the quadratic coefficient a_r is -0.001125 . In other words, the maximum contact stress without edge contact is not less than 758.36 MPa as each group of modification parameters is in the intervals of $u_0 \in [-1, 2]$ and $a_r \in [-0.01, 0.01]$.

Table 3. Results of the optimization calculation for the modified helical face gear.

Parameter	Value
Optimal parabola offset distance u_0 (mm)	1.6406
Optimal quadratic coefficient a_r	−0.001125
The optimized value of maximum contact stress P_{0_min} (MPa)	758.36

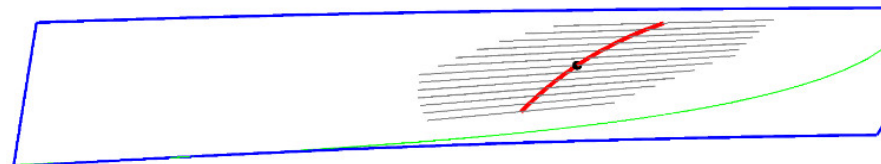


Figure 11. The optimized contact diagram (gray shades: contact area; red line: contact path; black point: maximum contact stress; green line: transition curve; blue lines: tooth borders).

Based on the optimization model, the contact path on the tooth surface of the face gear corresponding to the parameters in Table 1 can be obtained, as shown in Figure 11.

The edge contact has been avoided, and the contact area and contact path have also changed. Compared with the result before optimization (as shown in Figure 8), the optimized contact area and contact path are more inclined, and the contact path is longer, which is conducive to improving the contact ratio and transmission stability. Moreover, the contact area is further away from the inner portion of the face gear, reducing the risk of edge contact.

4.3. Verification of the Optimization Model

In order to further verify the effect of the proposed optimization model, some numerical calculations are carried out. The optimization effect to be verified includes three aspects: avoiding edge contact, minimizing the maximum contact stress, and efficiency.

As shown in Figure 11, the effect of the proposed model in avoiding edge contact is obvious. To verify the effect of the proposed model in minimizing the maximum contact stress, the contact stress values of different parameters in the intervals of $u_0 \in [-1, 2]$ and $a_r \in [-0.01, 0.01]$ are calculated by permutation and combination and are shown in Tables 4 and 5.

Table 4. Contact stress of different parabola offset distances u_0 .

Contact Case Number	u_0 (mm)	a_r	Maximum Contact Stress (MPa)
1	−1	−0.001125	Edge contact
2	0.7	−0.001125	Edge contact
3	1.5	−0.001125	Edge contact
4	1.64	−0.001125	758.36
5	1.70	−0.001125	758.52
6	1.75	−0.001125	758.66
7	1.80	−0.001125	758.77
8	1.85	−0.001125	758.93
9	1.90	−0.001125	759.07
10	2	−0.001125	759.34

All values of the maximum contact stresses in Tables 4 and 5, except for the cases of edge contact (which will not be displayed in the optimization results), are greater than 758.36 MPa, which means that the optimization algorithm minimizes the maximum contact

stress. According to the data in Tables 4 and 5, when the value of parameter u_0 becomes relatively small, or the absolute value of coefficient a_r becomes relatively large, edge contact is easily prone to emerge.

Table 5. Contact stress of different parabolic parameters a_r .

Contact Case Number	u_0 (mm)	a_r	Maximum Contact Stress (MPa)
1	1.6406	−0.01	Edge contact
2	1.6406	−0.002	Edge contact
3	1.6406	−0.0015	Edge contact
4	1.6406	−0.001	765.81
5	1.6406	−0.0005	777.38
6	1.6406	0	790.78
7	1.6406	0.002	841.65
8	1.6406	0.0022	844.77
9	1.6406	0.003	Edge contact
10	1.6406	0.008	Edge contact

The parameter ranges are $u_0 \in [-1, 2]$ and $a_r \in [-0.01, 0.01]$. The step size of parameter u_0 is 0.1, and the step size of parameter a_r is 0.001. Thus, there are 31×21 groups of modification parameters as a selection. For each group of parameters, the maximum value of the contact stress is selected from the values of contact stress at all contact points. The minimum is selected from these maximum values as the result of optimization that demotes the optimal values. In Tables 4 and 5, 21 sets of data are presented which are the most representative of the two dimensions. Hence, these sets of data supporting the conclusion are considered credible. According to Table 6, the proposed optimization model improves the efficiency by 10%, and the simplified TCA equation makes the algorithm more stable and less sensitive to the initial values of the numerical calculation.

Table 6. Comparison of the computation efficiency of two optimization models.

Computation Environment	The Computation Time of the Conventional Model	The Computation Time of the Proposed Model
MATLAB R2014a Run on a computer with 64-bit Intel Core i5-8400M 2.81 GHz CPU and 8 GB main memory	14.78 s	13.24 s
MATLAB R2014a Run on a laptop with 64-bit AMD A8-4500M 1.9 GHz CPU and 4 GB main memory	75.27 s	63.26 s

5. Discussion

In this section, the optimization model is applied to further analyze the effects of design parameters and assembly errors on the contact path and the contact stress.

5.1. The Effect of Modification on Contact Stress and Contact Path

As known to all, the purpose of the modification of gears is to improve contact performance. By comparing the contact performances of a modified face gear and an unmodified one, the influence of the modification on gear transmission can be studied. When the quadratic coefficient a_r of the modification parabola is equal to 0, the enveloped helical face gear can be regarded as a standard gear without modification. According to the

design parameters in Table 1, the contact path of the standard helical face gear is presented in Figure 12.

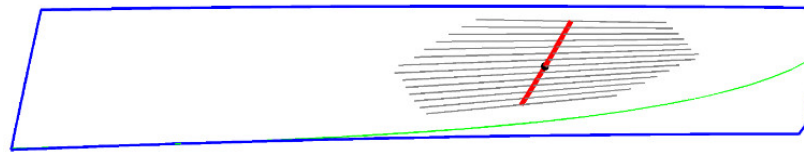


Figure 12. Contact diagram of the helical face gear without modification ($a_r = 0$).

According to the constraints in Equation (10), the edge contact could be avoided even if there is no modification. The optimized result of the maximum contact stress of the unmodified helical face gear is shown in Table 7 based on Equation (12).

Table 7. Optimization result of the helical face gear without modification.

Parameter	Value
Optimal parabola offset distance u_0 (mm)	-
Optimal quadratic coefficient of the parabola a_r	0
The minimum value of maximum contact stress P_{0m} (MPa)	790.78

As shown in Figures 11 and 12, the contact path of the unmodified helical face gear tends to be a straight line, while the contact path with modification is a smooth curve. The position of the maximum contact stress changes slightly. In addition, the contact area of the modified helical face gear is more inclined than that of the unmodified one and is closer to the inner portion of the face gear. The maximum contact stress of the unmodified helical face gear is 790.78 MPa, and that of the modified one is 758.36 MPa. Thus, the conclusion can be drawn that the modification expands the contact path and reduces the maximum contact stress, which indicates the necessity of the parabolic modification of the helical face gear.

5.2. The Effect of the Tooth Number Difference between a Shaper and a Pinion on Contact Stress and Contact Path

According to the meshing theory of the face gear drive, the tooth number of a shaper is 1 to 3 larger than that of a pinion. The surface geometry of the pinions with different tooth numbers is extremely distinct, which results in the fact that the geometry of the contact ellipses varies when the pinions are contacting with helical face gears. The optimization results for the face gear drives with different tooth numbers are listed in Table 8.

Table 8. Optimization results for different tooth numbers.

Case	Z_s/Z_1	Tooth Difference	u_0 (mm)	a_r	P_{0m} (MPa)
1	28/25	3	1.6406	-0.001125	758.36
2	28/26	2	1.7295	-0.000757	686.51
3	27/25	2	1.0063	-0.000815	703.72
4	28/27	1	0.0344	-0.000266	591.56
5	27/26	1	1.2893	-0.000336	609.60
6	26/25	1	1.5438	-0.000250	634.50

Figure 13 shows the contact paths on the tooth surface of the face gear under different tooth-number differences between the pinion and the shaper, namely cases 1, 2, and 4 in Table 8. The three curves in Figure 13 are all generated by the 28-tooth shaper. Thus, the influence of the minor change in modification parameters on the tooth geometry of the face gear is ignored.

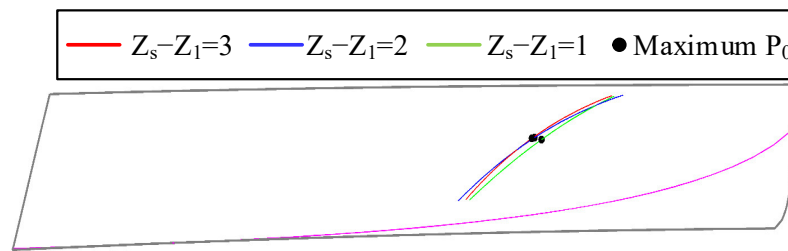


Figure 13. Contact paths of different tooth-number differences between the shaper and the pinion.

Results in Table 8 denote that the optimal modification coefficients of helical face gears continuously vary as the tooth numbers of the shaper and the pinion distinctly change. The optimal maximum contact stress is 758.36 MPa when the tooth number difference between the shaper and the pinion is 3. When the tooth number difference is 2, the contact stresses are 686.51 MPa and 703.72 MPa. As for the cases where the tooth number difference is 1, the stresses are 591.56 MPa, 609.60 MPa, and 634.5 MPa, respectively. As a result, the greater the tooth number difference is, the larger the optimal maximum contact stress is.

The contact paths of the modified helical face gears are different when the tooth number difference changes under the condition that the tooth number of the shaper is identical, as Figure 13 shows. As the tooth number difference increases, the contact path slightly moves towards the outer portion of the face gear. Additionally, the point of the maximum contact stress on the surface of the face gear remains the same tooth height.

5.3. The Effect of Pressure Angle α_n on Contact Stress and Contact Path

The inclination of the involute is related to the pressure angle which influences the contact path and the contact stress of face gear drives by changing the direction of the contact force. Some pressure angles as well as the corresponding optimization results are listed in Table 9.

Table 9. Optimization results for different pressure angles α_n .

α_n (°)	u_0 (mm)	a_r	P_{0m} (MPa)
22.5	1.3344	-0.001125	811.27
20	-0.9965	0.000501	912.73
17.5	Edge contact		
14.5	Edge contact		

The contact paths corresponding to different pressure angles in Table 9 are shown in Figure 14. In Tables 4 and 9, as the pressure angle α_n decreases from 25° to 20°, the optimal modification parameters change constantly, and the optimal maximum contact stress increases from 758.36 MPa to 912.73 MPa. Within the given ranges of modification parameters, namely $u_0 \in [-1, 2]$ and $a_r \in [-0.01, 0.01]$, the edge contact is inevitable if the pressure angle is equal to or less than 17.5°. Hence, the smaller the pressure angle within the certain range is, the greater the optimal maximum contact stress is.

When the pressure angle α_n decreases from 25° to 20° (as shown in Figures 11 and 14), the contact area on the surfaces of the face gears that adopt optimal modification parameters gradually moves to the inner portion of the face gears, the shapes of the contact area change from oblique distribution to longitudinal distribution, and the contact path also changes from oblique lines of the tooth root to vertical lines. Meanwhile, the point of the maximum contact stress keeps working in the middle of the contact path. Therefore, the angle of 25° is the most appropriate of the given pressure angles, which is why many aviation gears are designed with a pressure angle of 25°.

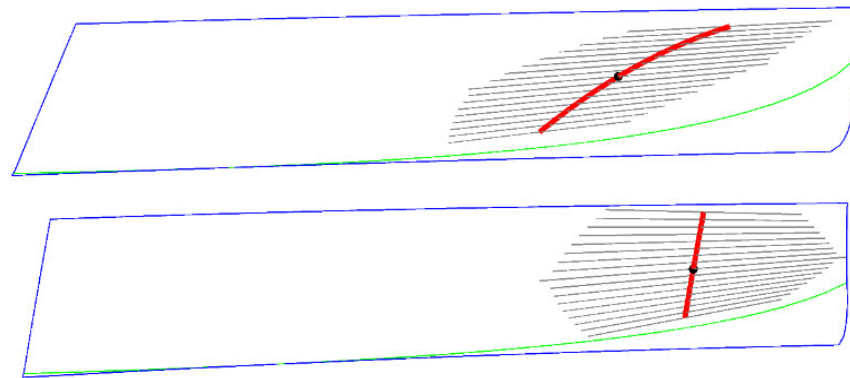


Figure 14. Contact diagrams of the helical face gears with different pressure angles (above: $\alpha_n = 22.5^\circ$; below: $\alpha_n = 20^\circ$).

5.4. The Effect of Helical Angle β on Contact Stress and Contact Path

The helical angle determines the helical torsion degree of the tooth around the gear axis, which inevitably affects the distribution of the contact area on the tooth surface. As a result, helical angles can further change the contact path and contact stress. Some optimized maximum contact stresses of modified helical face gears with different helical angles are shown in Table 10.

Table 10. Optimization results for different helical angles β .

β ($^\circ$)	u_0 (mm)	a_r	P_{0m} (MPa)
0	−0.3000	0	805.53
5	−0.5468	−0.000279	806.78
10	1.8453	−0.001063	755.02
21	1.9775	0.001951	845.13

To obtain the influence laws of helical angles on the contact characteristics of face gears, the contact paths and contact areas corresponding to different helical angles are compared and shown in Figure 15.

According to the results in Tables 4 and 10, as the helical angle β increases from 0° to 21° , the optimal modification parameters and the values of the optimal maximum contact stress gradually vary. When the helical angle β is between 10° and 15° , the optimal modification coefficient u_0 is close to the maximum value of the given range, that is, $u_0 \in [-1, 2]$. The parameter a_r is close to the minimum value in the given range of $a_r \in [-0.01, 0.01]$, while the optimal result of the maximum contact stress is around the minimum value of 755.02 MPa. According to Figures 11 and 15, the following conclusions can be drawn as the helical angle β increases from 0° to 21° : (i) The position of the contact area on the tooth surface of the face gear moves inward gradually. (ii) The tilt of the contact area increases gradually. (iii) The contact path gradually changes from a vertical line of the tooth root to an inclined line which will improve the contact ratio. (iv) The point of the maximum contact stress on the face gear surface slightly shifts towards the tooth height. Therefore, it can be concluded that the helical angle has a significant influence on the contact characteristics. As for the modified helical face gear drives with the parameters listed in Table 1, the helical angles of 10° to 15° are considered relatively ideal parameters with the comprehensive consideration of the contact stress and the distribution of the contact area.

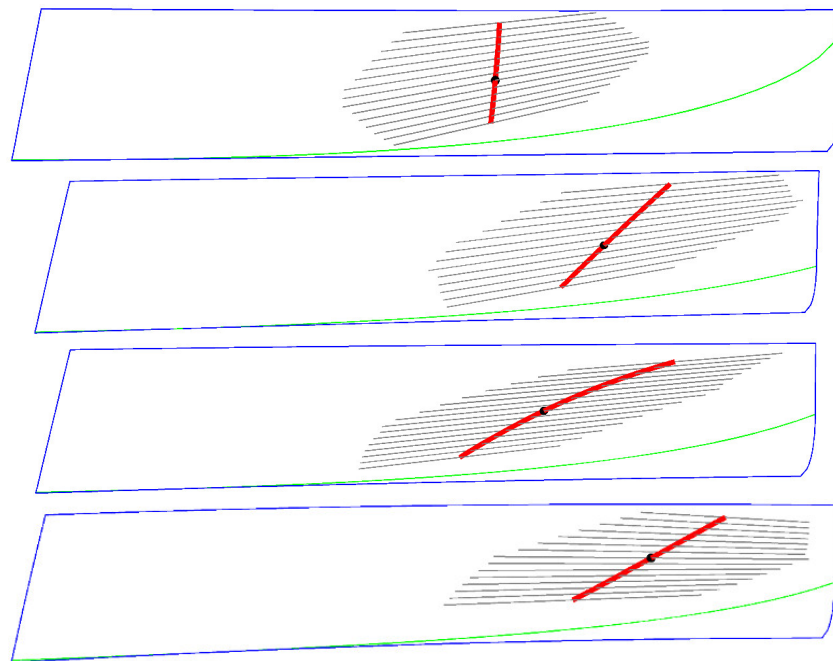


Figure 15. Contact diagrams of different helical angles (first: $\beta = 0^\circ$; second: $\beta = 5^\circ$; third: $\beta = 10^\circ$; fourth: $\beta = 21^\circ$).

5.5. The Effect of Shaft Angle γ_m on Contact Stress and Contact Path

In Table 11, different shaft angles and the corresponding optimal maximum contact stresses are illustrated.

Table 11. Optimization results for different shaft angles γ_m .

γ_m ($^\circ$)	u_0 (mm)	a_r	P_{0m} (MPa)
80	-0.8136	-0.000585	688.07
90	-0.8453	-0.000950	757.42
110	-0.0505	-0.000688	685.11

Similarly, the contact paths and contact areas that are associated with the shaft angles in Table 11 are separately shown in Figure 16.

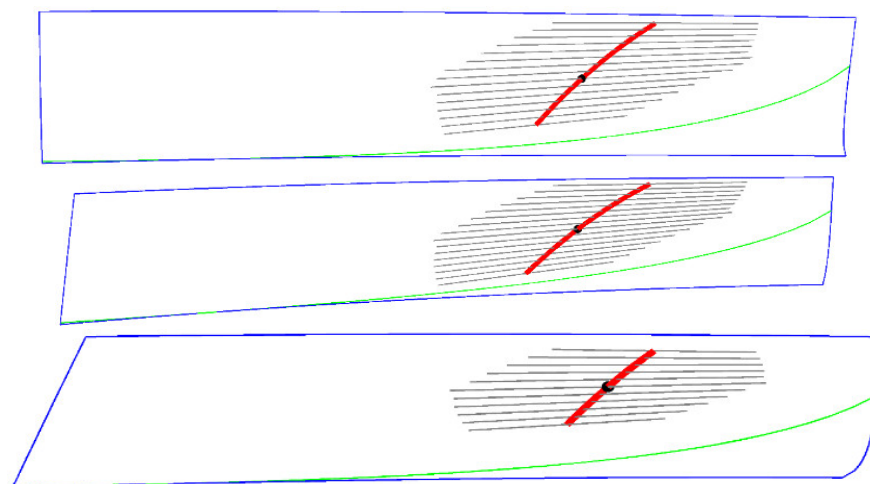


Figure 16. Contact diagrams of different shaft angles (above: $\gamma_m = 80^\circ$; middle: $\gamma_m = 90^\circ$; below: $\gamma_m = 110^\circ$).

The data in Tables 4 and 11 indicate that the tooth surfaces of the modified face gears with different shaft angles are dramatically distinct, and so are the corresponding optimal modification parameters. If the shaft angle is close to 90°, the value of the maximum contact stress reaches the maximum, which is about 760 MPa. According to Figures 11 and 16, as the shaft angle changes from 80° to 110°, the positions of the contact path and the maximum contact stress point on the tooth surface of the face gear do not change obviously. However, the shapes of the contact area are much too diverse. Generally, the contact length would increase as soon as the contact area is tilted, which is beneficial for improving the contact ratio. According to a previous comprehensive analysis of contact stress and contact area, the recommended value of shaft angle γ_m for this design is about 100°.

The influence laws of the shaft angle error $\Delta\gamma_m$ on the contact path and the contact stress are consistent with those of the shaft angle γ_m , which will not be repeatedly mentioned here.

5.6. The Effects of Assembly Errors Δq and ΔE on Contact Stress and Contact Path

It cannot be ignored that assembly errors have a great impact on the contact characteristics of the modified helical face gear, the investigation of which provides significant references for the practical assembly. In Table 12, axial displacement errors and the corresponding optimal maximum contact stresses are listed, and the contact paths in Figure 17 correspond to the parameters in Table 12.

Table 12. Optimization results for different axial displacement errors Δq .

Δq (mm)	u_0 (mm)	a_r	P_{0m} (MPa)
0	1.6406	−0.001125	758.36
0.03	−0.8997	−0.001	751.38
0.05	−0.2787	−0.001117	746.55
0.08	−0.7123	−0.001086	742.19

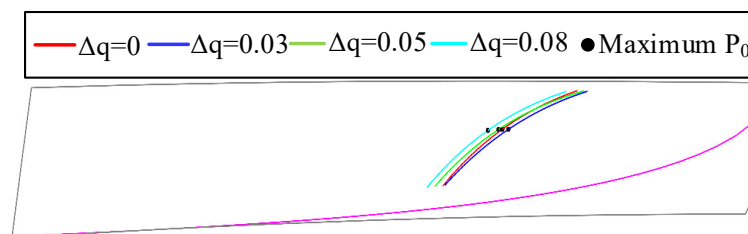


Figure 17. Contact paths for different values of the axial displacement error.

Similarly, the different cases of the modified helical face gear drive with offset errors ΔE are presented in Table 13 and Figure 18.

Table 13. Optimization results for different values of pinion-offset error ΔE .

ΔE (mm)	u_0 (mm)	a_r	P_{0m} (MPa)
0.02	−0.1190	−0.001081	756.51
0.08	0.6547	−0.001063	767.60
0.15	0.8649	−0.000758	680.87
0.25	1.1063	−0.000813	797.86

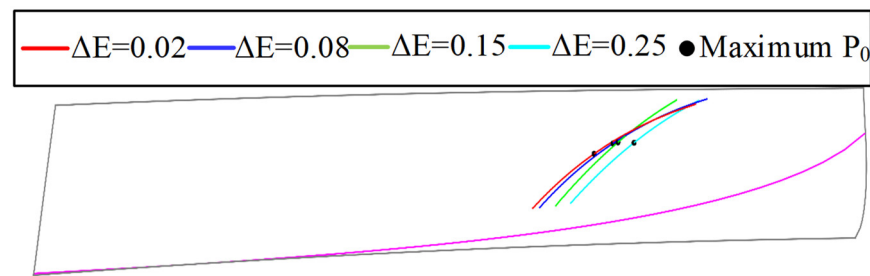


Figure 18. Contact paths of the modified helical face gears with different pinion-offset errors.

As Table 12 indicates, as the axial displacement error Δq gradually increases from 0 to 0.08 mm, the optimal modification coefficient u_0 changes from 1.6406 mm to -0.7123 mm. Accordingly, the quadratic coefficient a_r also changes from -0.001125 to -0.001086 , and the optimized maximum contact stress is close to 758.36 MPa. As shown in Figure 17, the contact paths on the tooth surface of the face gear evidently move toward the middle area as the assembly error grows, which decreases the risks of edge contact. The points of the maximum contact stress on the gear surface do not change significantly and remain at the same tooth height. Thus, in actual installations, the displacement error Δq is recommended to be controlled within the range of 0.08 mm, and the contact performance of the modified face gear is relatively ideal.

As shown in Table 13, the pinion offset ΔE greatly influences the optimal modification coefficients and the contact stresses of the modified face gear drive. As the offset value grows from 0.02 mm to 0.25 mm, the optimum modification parameter u_0 correspondingly varies from -0.1190 mm to 1.1063 mm, and the coefficient a_r also changes from -0.001081 to -0.000813 , which results in the fluctuation of the maximum contact stresses. Figure 18 reveals that the gradual increase in the offset values causes the contact paths to move to the inner portion of the face gear and also causes the point of the maximum contact stress to move along the direction of tooth height. In other words, the addition of offset ΔE increases the risks of edge contact. When the offset ΔE is equal to 0.15 mm, the maximum contact stress is 680.87 MPa, which is the smallest in the given range. In this case, the contact path is reasonable. In summary, the recommended value of the offset error ΔE is 0.15 mm, taking into account the inevitability of assembly errors.

6. Conclusions

An ELTCA model for optimizing contact stress and edge contact is presented and verified in this paper. Based on the above research, the following conclusions can be drawn.

- (1) The proposed ELTCA optimization model can determine the optimal modification parameters for avoiding edge contact and minimizing the maximum contact stress programmatically.
- (2) The parabolic modification of the helical face gear is beneficial for improving the contact performance, expanding the contact areas, and reducing the maximum contact stress.
- (3) The tooth number difference between the shaper and the pinion has great effects on the optimal modification parameters. The increase in tooth number difference contributes to an increase in the values of the maximum contact stress. However, the change in the relative position of the point of maximum contact stress on the contact path is small.
- (4) The pressure angle α_n , the shaft angle γ_m , and the helical angle β affect the contact path and the maximum contact stress in different degrees of influence. For specific design parameters of helical face gear drives, these three kinds of angles have relatively ideal values or ranges, which can optimize the contact stress and contact path.

Within a small range, the axial displacement error Δq can improve the contact performance, while the pinion offset ΔE worsens the contact performance. The influence of the shaft angle error $\Delta \gamma_m$ on the contact performance is similar to that of shaft angle γ_m , but the influence degree is distinct.

Author Contributions: Conceptualization, S.W. and Z.W.; methodology, B.H.; software, B.H.; validation, Y.Z.; formal analysis, S.W.; investigation, S.W., Z.W. and B.H.; resources, J.T.; data curation, Y.Z.; writing—original draft preparation, S.W.; writing—review and editing, S.W., B.H., Z.W. and Y.Z.; visualization, J.T.; supervision, Y.Z. and Z.W.; project administration, Y.Z.; funding acquisition, Y.Z. All authors have read and agreed to the published version of the manuscript.

Funding: The authors gratefully acknowledge the support from the National Key R&D Program of China (No. 2018YFB2001700); the Project of State Key Laboratory of High Performance Complex Manufacturing, Central South University (No. ZZYJKT2020-06); Industrial Technology Development Program (No. JCKY2020213B006); Hunan Provincial Natural Science Foundation of China (No. 2021JJ20071); Innovation Platform and Talent Plan of Hunan Province (No. 2021RC3012) and Guizhou Provincial Science and Technology Projects (No. ZK2022-209).

Institutional Review Board Statement: Not applicable.

Informed Consent Statement: Not applicable.

Data Availability Statement: The data presented in this study are available from the corresponding author on request.

Conflicts of Interest: The authors declare no conflict of interest.

References

- Litvin, F.L.; Zhang, Y.; Wang, J.C.; Bossler, R.B.; Chen, Y.J.D. Design and geometry of face-gear drives. *J. Mech. Des.* **1992**, *114*, 642–647. [[CrossRef](#)]
- Litvin, F.; Egelja, A.; Tan, J.; Heath, G. Computerized design, generation and simulation of meshing of orthogonal offset face-gear drive with a spur involute pinion with localized bearing contact. *Mech. Mach. Theory* **1998**, *33*, 87–102. [[CrossRef](#)]
- Litvin, F.L.; Fuentes, A.; Zanzi, C.; Pontiggia, M.; Handschuh, R.F. Face-gear drive with spur involute pinion: Geometry, generation by a worm, stress analysis. *Comput. Methods Appl. Mech. Eng.* **2002**, *191*, 2785–2813. [[CrossRef](#)]
- Litvin, F.L.; Gonzalez-Perez, I.; Fuentes, A.; Vecchiato, D.; Hansen, B.D.; Binney, D. Design, generation and stress analysis of face-gear drive with helical pinion. *Comput. Methods Appl. Mech. Eng.* **2005**, *194*, 3870–3901. [[CrossRef](#)]
- Litvin, F.L.; Nava, A.; Fan, Q.; Fuentes, A. New geometry of face worm gear drives with conical and cylindrical worms: Generation, simulation of meshing, and stress analysis. *Comput. Methods Appl. Mech. Eng.* **2002**, *191*, 3035–3054. [[CrossRef](#)]
- Litvin, F.L.; Fuentes, A.; Gonzalez-Perez, I.; Piscopo, A.; Ruzziconi, P. *Face Gear Drive with Helical Involute Pinion: Geometry, Generation by a Shaper and a Worm, Avoidance of Singularities and Stress Analysis*; Tanzania Journal of Health Research: Tanzania, East Africa, 2005.
- Litvin, F.L.; Egelja, A.; Tan, J.; Chen, D.Y.D.; Heath, G. *Handbook on Face Gear Drives with a Spur Involute Pinion*; NASA/CR-2000-209909; NASA: Washington, WA, USA, 2000.
- Litvin, F.L. *Gear Geometry and Applied Theory*; Prentice-Hall: Hoboken, NJ, USA, 1994.
- Wang, Y.; Su, G.; Chu, X.; Huang, Y.; Shiyuan, E.; Zhang, W.; Liu, Y. A finishing method for the continuous generation of spur face gears with shaving cutters. *Int. J. Mech. Sci.* **2020**, *190*, 106020. [[CrossRef](#)]
- He, C.; Lin, C. Analysis of loaded characteristics of helical curve face gear. *Mech. Mach. Theory* **2017**, *115*, 267–282. [[CrossRef](#)]
- Mo, S.; Song, W.; Zhu, S.; Feng, Z.; Tang, W.; Gao, H. Complex geometric modeling and tooth contact analysis of a helical face gear pair with arc-tooth. *J. Cent. South Univ.* **2022**, *29*, 1213–1225. [[CrossRef](#)]
- Tang, Z.; Zhou, Y.; Wang, S.; Zhu, J.; Tang, J. An innovative geometric error compensation of the multi-axis CNC machine tools with non-rotary cutters to the accurate worm grinding of spur face gears. *Mech. Mach. Theory* **2022**, *169*, 104664. [[CrossRef](#)]
- Zhou, Y.; Tang, Z.; Shi, X.; Tang, J.; Li, Z. Efficient and accurate worm grinding of spur face gears according to an advanced geometrical analysis and a closed-loop manufacturing process. *J. Cent. South Univ.* **2022**, *29*, 1–13. [[CrossRef](#)]
- Lu, X.; Zhou, Y.; He, D.; Zheng, F.; Tang, K.; Tang, J. A novel two-variable optimization algorithm of TCA for the design of face gear drives. *Mech. Mach. Theory* **2022**, *175*, 104960. [[CrossRef](#)]
- Yang, X.-y.; Tang, J.-y. Research on manufacturing method of CNC plunge milling for spur face-gear. *J. Mater. Process. Technol.* **2014**, *214*, 3013–3019. [[CrossRef](#)]
- Tang, J.; Yang, X. Research on manufacturing method of planing for spur face-gear with 4-axis CNC planer. *Int. J. Adv. Manuf. Technol.* **2015**, *82*, 847–858. [[CrossRef](#)]
- Wang, S.; Zhou, Y.; Tang, J.; Tang, K.; Li, Z. Digital tooth contact analysis of face gear drives with an accurate measurement model of face gear tooth surface inspected by CMMs. *Mech. Mach. Theory* **2022**, *167*, 104498. [[CrossRef](#)]

18. Liu, D.; Ren, T.; Jin, X. Geometrical model and tooth analysis of undulating face gear. *Mech. Mach. Theory* **2015**, *86*, 140–155. [[CrossRef](#)]
19. Zschippang, H.A.; Weikert, S.; Küçük, K.A.; Wegener, K. Face-gear drive: Geometry generation and tooth contact analysis. *Mech. Mach. Theory* **2019**, *142*, 103576. [[CrossRef](#)]
20. Tan, J. Face gearing with a conical involute pinion: Part 1. The conical involute gear: Definition, geometry and generation. In Proceedings of the ASME 2002 Design Engineering Technical Conferences and Computer and Information in Engineering Conference, Montreal, QC, Canada, 29 September–2 October 2002.
21. Tan, J. Face gearing with a conical involute pinion: Part 2. The face gear-meshing with the pinion, tooth geometry and generation. In Proceedings of the ASME 2003 Design Engineering Technical Conferences and Computers and Information in Engineering Conference, Chicago, IL, USA, 2–6 September 2003.
22. Tan, J. Face Gearing with Conical Involute Pinion. U.S. Patent 005941124A, 24 August 1999.
23. Li, Z.; Wu, H.; Zhu, R. Influence predictions of geometric parameters on face gear strength. *Adv. Mech. Eng.* **2015**, *7*, 1–7. [[CrossRef](#)]
24. Lin, C.; He, C.; Hu, Y. Analysis on the kinematical characteristics of compound motion curve-face gear pair. *Mech. Mach. Theory* **2018**, *128*, 298–313. [[CrossRef](#)]
25. Cai, Z.; Lin, C. Research on the discrete algorithm of tooth surface for a curve-face gear. *J. Mech. Des.* **2020**, *142*, 053301. [[CrossRef](#)]
26. Zhang, Y.; Wu, Z. Offset face gear drives: Tooth geometry and contact analysis. *J. Mech. Des.* **1997**, *119*, 114–119. [[CrossRef](#)]
27. Guo, H.; Gonzalez-Perez, I.; Fuentes-Aznar, A. Computerized generation and meshing simulation of face gear drives manufactured by circular cutters. *Mech. Mach. Theory* **2019**, *133*, 44–63. [[CrossRef](#)]
28. Litvin, F.L.; Fuentes, A.; Zanzi, C.; Pontiggia, M. Design, generation, and stress analysis of two versions of geometry of face-gear drives. *Mech. Mach. Theory* **2002**, *37*, 1179–1211. [[CrossRef](#)]
29. Litvin, F.L.; Fuentes, A.; Howkins, M. Design, generation and TCA of new type of asymmetric face-gear drive with modified geometry. *Comput. Methods Appl. Mech. Eng.* **2001**, *190*, 5837–5865. [[CrossRef](#)]
30. Wu, C.; Cao, P. The application of tooth contact analysis in the shaper modification for face-gear. *Procedia Eng.* **2015**, *99*, 94–100. [[CrossRef](#)]
31. Barone, S.; Borgianni, L.; Forte, P. Evaluation of the effect of misalignment and profile modification in face gear drive by a finite element meshing simulation. *J. Mech. Des.* **2004**, *126*, 916–924. [[CrossRef](#)]
32. Peng, X.; Zhang, L.; Fang, Z. Manufacturing process for a face gear drive with local bearing contact and controllable unloaded meshing performance based on ease-off surface modification. *J. Mech. Des.* **2016**, *138*, 043302. [[CrossRef](#)]
33. Zanzi, C.; Pedrero, J. Application of modified geometry of face gear drive. *Comput. Methods Appl. Mech. Eng.* **2005**, *194*, 3047–3066. [[CrossRef](#)]
34. Dong, J.; Tang, J.; Hu, Z. Investigation of assembly, power direction and load sharing in concentric face gear split-torque transmission system. *Meccanica* **2019**, *54*, 2485–2506. [[CrossRef](#)]
35. Dong, J.; Tang, J.; Hu, Z.; Wang, Y. A semi-analytical method of time-varying mesh stiffness in concentric face gear split-torque transmission system. *J. Mech. Sci. Technol.* **2020**, *34*, 589–602. [[CrossRef](#)]
36. Mo, S.; Zhang, Y.; Luo, B.; Bao, H.; Cen, G.; Huang, Y. The global behavior evolution of non-orthogonal face gear-bearing transmission system. *Mech. Mach. Theory* **2022**, *175*, 104969. [[CrossRef](#)]
37. Mo, S.; Luo, B.; Song, W.; Zhang, Y.; Cen, G.; Bao, H. Geometry design and tooth contact analysis of non-orthogonal asymmetric helical face gear drives. *Mech. Mach. Theory* **2022**, *173*, 104831. [[CrossRef](#)]
38. Liu, C.; Shi, W.; Curá, F.; Mura, A. A novel method to predict static transmission error for spur gear pair based on accuracy grade. *J. Cent. South Univ.* **2020**, *27*, 3334–3349. [[CrossRef](#)]
39. Johnson, K.L. *Contact Mechanics*; Higher Education Press: Beijing, China, 1985. (In Chinese)